Supplementary Figure S1: Reconstruction of simulated dipoles.

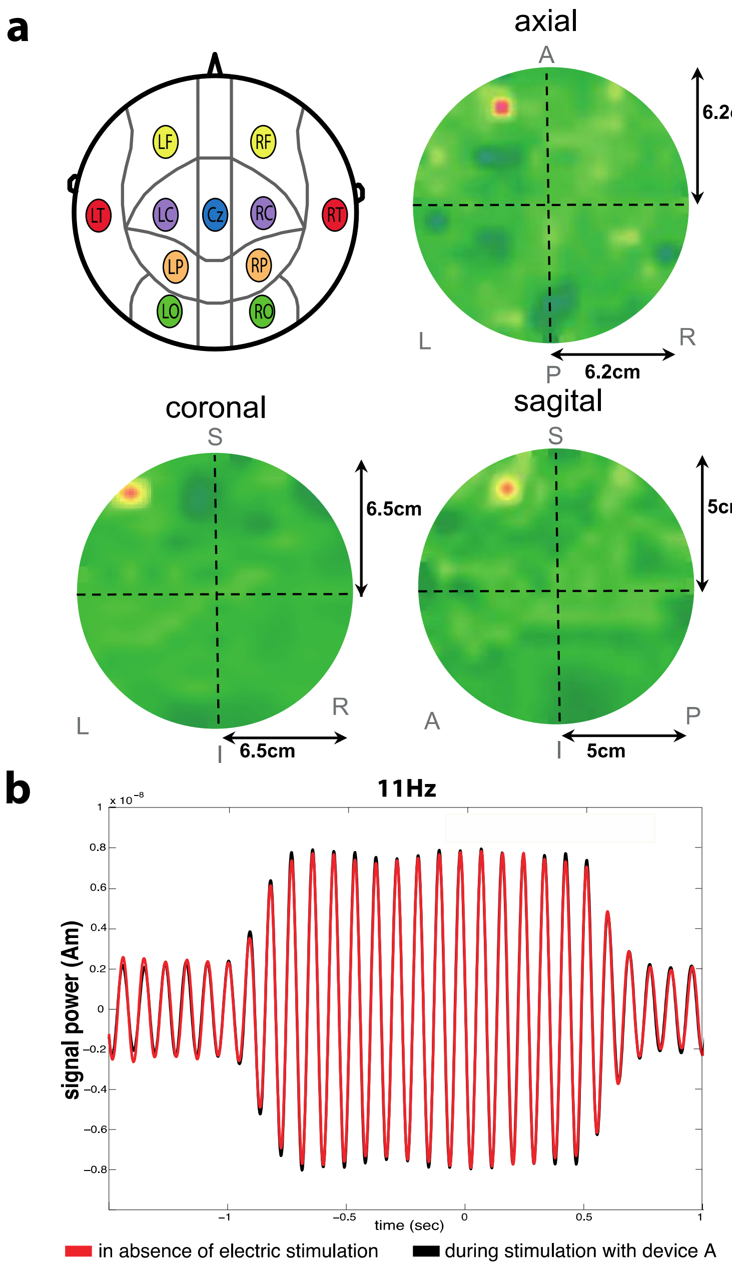

For validation of generalizability of the results at other head locations, 11 simulated dipoles were embedded into the interference data recorded in the presence of tDCS (a). Reconstruction resulted in accurate localization and reconstruction of all simulated dipoles (Supplementary Table S1), e.g. at locations LF illustrated in (b).

Supplementary Table 1: Coherence of signal reconstruction of simulated dipoles (11Hz) at 11 different head locations.

Location	Simulated coordinates			Localized coordinates in absence of tDCS (mm)			Localized coordinates during stimulation with device A (mm)			Coherence
	x	*y*	*z*	*x*	*y*	*z*	*x*	*y*	*z*	
CZ	*0*	*0*	*7*	*0*	*0*	*7*	*0*	*0*	*7*	0,9998
LF	*6*	*3*	*6*	*6*	*3*	*6*	*6*	*3*	*6*	0,9995
RF	*6*	*-3*	*6*	*6*	*-3*	*6*	*6*	*-3*	*6*	0,9996
LC	*0*	*3*	*7*	*0*	*3*	*7*	*0*	*3*	*7*	0,9996
RC	*0*	*-3*	*7*	*0*	*-3*	*7*	*0*	*-3*	*7*	0,9902
LT	*0*	*6*	*5*	*0*	*6*	*5*	*0*	*6*	*5*	0,9981
RT	*0*	*-6*	*5*	*0*	*-6*	*5*	*0*	*-6*	*5*	0,9916
LP	*-3*	*3*	*6*	*-3*	*3*	*6*	*-3*	*3*	*6*	0,9996
RP	*-3*	*-3*	*6*	*-3*	*-3*	*6*	*-3*	*-3*	*6*	0,9996
LO	*-6*	*4*	*4*	*-6*	*4*	*4*	*-6*	*4*	*4*	0,9958
RO	*-6*	*-4*	*4*	*-6*	*-4*	*4*	*-6*	*-4*	*4*	0,9905
mean coherence										0.9967 +/- 0.004

LF: left frontal; RF: right frontal; LC: left central; RC: right central; LT: left temporal; RT: right temporal; LP: left parietal; RP: right parietal; LO: left occipital; RO: right occipital.

Supplementary Methods

Source reconstruction using Synthetic Aperture Magnetometry (SAM)

Various mathematical approaches can be used to improve spatial accuracy of source reconstruction, for instance beamforming that combines noise cancellation features with source localization[61]. Synthetic Aperture Magnetometry (SAM)[30], a scalar linearly constrained minimum variance (LCMV) beamformer showed to be advantageous for suppressing external interferences compared to conventional dipole analysis techniques[62], and is capable of source localization despite MEG artifacts, for instance due to metallic orthodontic implants or fillings[63]. SAM acts as a spatial filter for estimating cortical source activity on a voxel by voxel basis, thereby generating functional brain images, for example, of oscillatory power. The spatial filter minimizes all signals except for that arising from specified spatial locations, resulting in noise cancellation of other biomagnetic signals such as muscular artifacts due to eye movements, cardiac or respiratory activity.

For SAM analysis, a linear projection of sensor data using a spatial filter computed from the lead field (L) of the source of interest and the data covariance matrix was used[30]. Assuming a unitary current dipole located at a given position (θ) and orientation, L represents the field distribution across the whole MEG sensor array. Accordingly, the beamformer output $y_{\boldsymbol{\theta}}$ at the location q is defined as the weighted sum of the measured signals from all sensors (1). Given a sufficient number of time samples, an instantaneous source estimate $\tilde{P}_{\boldsymbol{\theta}}$ for coordinate q was constructed as the weighted sum MEG measurements.

$$\tilde{P}_{\boldsymbol{\theta}} = \boldsymbol{W}_{\boldsymbol{\theta}}^{T}\boldsymbol{M}(k) \qquad (1)$$

M(k) represents the matrix of the magnetic field (in Tesla) at the sensor level at time sample k. $\boldsymbol{W}_{\boldsymbol{\theta}}^{T}$ is the weight matrix, determined by minimizing the power projected from location $\boldsymbol{\theta}$ (2).

$$P_{\boldsymbol{\theta}}^{2} = \boldsymbol{W}_{\boldsymbol{\theta}}^{T}\boldsymbol{C}\boldsymbol{W}_{\boldsymbol{\theta}} \qquad (2)$$

where **C** is the covariance matrix computed over the integration of time:

$$\boldsymbol{C} = <\boldsymbol{B}\boldsymbol{B}^T> \qquad (3)$$

where <.> denotes the expectation value. We solve for **W** by introducing a constraint such that $\boldsymbol{P}_{\boldsymbol{\theta}}^2$ (power or variance) is minimized subject to unit gain for a specified coordinate. One such constraint is:

$$\boldsymbol{W}_{\boldsymbol{\theta}}^T \boldsymbol{H}_{\boldsymbol{\theta}} = \mathbf{1} \qquad (4)$$

where $\boldsymbol{H}_{\boldsymbol{\theta}}$ is the a priori forward solution for the field observed by an array of M sensors generated by a current dipole source located at $\boldsymbol{\theta}$. That is:

$$\boldsymbol{H}_{\boldsymbol{\theta}} = \begin{bmatrix} \hbar_1(\boldsymbol{\theta}) \\ \hbar_2(\boldsymbol{\theta}) \\ \vdots \\ \hbar_M(\boldsymbol{\theta}) \end{bmatrix} \qquad (5)$$

A single sphere model[64] was used to compute the lead field L in experiments involving the phantom head. In all other experiments a realistic head model as described in Nolte et al.[65] was used.

However, to compute $\boldsymbol{H}_{\boldsymbol{\theta}}$ we must first estimate the dipole orientation. We do this by finding the dipole orientation yielding the highest signal-to-noise ratio (SNR) at location $\boldsymbol{\theta}$. We define $\boldsymbol{L}_{\boldsymbol{\theta}}$, the matrix of forward solutions for dipoles oriented in the three cardinal directions as:

$$\boldsymbol{L}_{\boldsymbol{\theta}} = \begin{pmatrix} \hbar_{11} & \hbar_{12} & \hbar_{13} \\ \hbar_{21} & \hbar_{22} & \hbar_{32} \\ \vdots & \vdots & \vdots \\ \hbar_{M1} & \hbar_{M2} & \hbar_{M3} \end{pmatrix} \qquad (6)$$

We also define a diagonal matrix Σ of uncorrelated sensor instrumental noise power σ_M^2:

$$\Sigma = \begin{bmatrix} \sigma_1^2 & & & 0 \\ & \sigma_2^2 & & \\ & & \ddots & \\ 0 & & & \sigma_M^2 \end{bmatrix} \qquad (7)$$

The source power **P** in each of three cardinal directions is given by:

$$\boldsymbol{P}_{\boldsymbol{\theta}}^2 = [\boldsymbol{L}_{\boldsymbol{\theta}}^T \boldsymbol{C}^{-1} \boldsymbol{L}_{\boldsymbol{\theta}}]^{-1} \qquad (8)$$

and the noise power **N** by:

$$\boldsymbol{N}_{\boldsymbol{\theta}}^2 = [\Sigma \boldsymbol{L}_{\boldsymbol{\theta}}^T \boldsymbol{C}^{-1} \boldsymbol{L}_{\boldsymbol{\theta}}]^{-1} \qquad (9)$$

The SNR is given by a generalized eigensystem of these two 3x3 matrices[66]. By assuming that the SQUID noise is nearly equal in all sensors, we can neglect Σ, as it represents a scalar that will not affect the determination of the moment vector.

The dipole orientation maximizing SNR is given by the eigenvector $\mathbf{e}_{\mathbf{max}}$ corresponding to the maximum eigenvalue λ_{max} of the generalized eigensystem:

$$\boldsymbol{L}_{\boldsymbol{\theta}}^T \boldsymbol{C}^{-2} \boldsymbol{L}_{\boldsymbol{\theta}} \boldsymbol{e}_k = \lambda_k \boldsymbol{L}_{\boldsymbol{\theta}}^T \boldsymbol{C}^{-\mathbf{1}} \boldsymbol{L}_{\boldsymbol{\theta}} \boldsymbol{e}_k \quad (10)$$

The forward solution for the dipole vector for the highest SNR is therefore:

$$\boldsymbol{H}_{\boldsymbol{\theta}} = \boldsymbol{L}_{\boldsymbol{\theta}} \boldsymbol{e}_{\boldsymbol{max}}$$

Solving for the optimum scalar LCMV beamformer weights using Lagrange multipliers results in:

$$\boldsymbol{W}_{\boldsymbol{\theta}} = \frac{\boldsymbol{C}^{-1} \boldsymbol{H}_{\boldsymbol{\theta}}}{\boldsymbol{H}_{\boldsymbol{\theta}}^T \boldsymbol{C}^{-\mathbf{1}} \boldsymbol{H}_{\boldsymbol{\theta}}} \qquad (11)$$

Substituting $\boldsymbol{W}_{\boldsymbol{\theta}}$ into Eq. 1 yields an estimate of the source time series.

Theoretical boundaries of TESANA

Localization and reconstruction of brain oscillations during applications of electric currents are limited by the dynamic recording range and maximum slew rate of the MEG system employed for neuromagnetic recordings. According to the manufacturer, the MEG system used in this investigation (CTF MEG® by MISL, Coquitlam, Canada) provides a maximum slew rate of 36.000 flux quantum (ϕ_0) per second. Equipped with a 20 bit A/D sensor gain, the maximum slew rate for this device translates as $6.13\text{x}10^3$ nT per second, leading to the following equation to calculate the maximum frequency of oscillating electric current stimulation:

$$6.13 \text{ x } 10^3 \ \frac{\text{nT}}{\text{sec}} = 2\pi\text{f x } H_{peak}$$

Where f is the frequency and H_{peak} is the peak magnetic field strength of the oscillating source. While this gives the theoretical boundaries of electric brain stimulation in this specific device, it is advisable not to exceed 70% of these limits to avoid flux trapping, and, if unknown, to inquire the maximum slew rates from the manufacturer.

Supplementary References

61. Brookes, M.J. *et al.* Source localisation in concurrent EEG/fMRI: applications at 7T. *Neuroimage* **45,** 440-452 (2009).
62. Brookes, M.J. *et al.* Optimising experimental design for MEG beamformer imaging. *Neuroimage* **39,** 1788-1802 (2008).
63. Cheyne, D., Bostan, A.C., Gaetz, W., Pang, E.W. Event-related beamforming: a robust method for presurgical functional mapping using MEG. *Clin Neurophysiol.* **118,** 1691-1704 (2007).
64. Hämäläinen, M., Sarvas, J. Realistic conductivity geometry model of the human head for interpretation of neuromagnetic data. *IEEE Trans Biomed Eng.* **36,** 165-171 (1989).
65. Nolte G., 2003. The magnetic lead field theorem in the quasi-static approximation and its use for magnetoencephalography forward calculation in realistic volume conductors. *Phys Med Biol.* **48,** 3637-3652 (2003).
66. Sekihara, K., Nagarajan, S.S., 2008. Scalar adaptive spatial filter: deriving the optimum source orientation in *Adaptive Spatial Filters for Electromagnetic Brain Imaging*, ed. J.H. Nagel, Springer (2008).